

NASA/TM—2018-219920



Jetting Phenomenon in Meshed Spur Gears

Irebert Delgado
Glenn Research Center, Cleveland, Ohio

Michael Hurrell
HX5 Sierra, LLC, Cleveland, Ohio

NASA STI Program . . . in Profile

Since its founding, NASA has been dedicated to the advancement of aeronautics and space science. The NASA Scientific and Technical Information (STI) Program plays a key part in helping NASA maintain this important role.

The NASA STI Program operates under the auspices of the Agency Chief Information Officer. It collects, organizes, provides for archiving, and disseminates NASA's STI. The NASA STI Program provides access to the NASA Technical Report Server—Registered (NTRS Reg) and NASA Technical Report Server—Public (NTRS) thus providing one of the largest collections of aeronautical and space science STI in the world. Results are published in both non-NASA channels and by NASA in the NASA STI Report Series, which includes the following report types:

- TECHNICAL PUBLICATION. Reports of completed research or a major significant phase of research that present the results of NASA programs and include extensive data or theoretical analysis. Includes compilations of significant scientific and technical data and information deemed to be of continuing reference value. NASA counter-part of peer-reviewed formal professional papers, but has less stringent limitations on manuscript length and extent of graphic presentations.
- TECHNICAL MEMORANDUM. Scientific and technical findings that are preliminary or of specialized interest, e.g., “quick-release” reports, working papers, and bibliographies that contain minimal annotation. Does not contain extensive analysis.
- CONTRACTOR REPORT. Scientific and technical findings by NASA-sponsored contractors and grantees.
- CONFERENCE PUBLICATION. Collected papers from scientific and technical conferences, symposia, seminars, or other meetings sponsored or co-sponsored by NASA.
- SPECIAL PUBLICATION. Scientific, technical, or historical information from NASA programs, projects, and missions, often concerned with subjects having substantial public interest.
- TECHNICAL TRANSLATION. English-language translations of foreign scientific and technical material pertinent to NASA's mission.

For more information about the NASA STI program, see the following:

- Access the NASA STI program home page at <http://www.sti.nasa.gov>
- E-mail your question to help@sti.nasa.gov
- Fax your question to the NASA STI Information Desk at 757-864-6500
- Telephone the NASA STI Information Desk at 757-864-9658
- Write to:
NASA STI Program
Mail Stop 148
NASA Langley Research Center
Hampton, VA 23681-2199

NASA/TM—2018-219920



Jetting Phenomenon in Meshed Spur Gears

Irebert Delgado
Glenn Research Center, Cleveland, Ohio

Michael Hurrell
HX5 Sierra, LLC, Cleveland, Ohio

Prepared for the
74th Annual Forum and Technology Display (Forum 74)
sponsored by the American Helicopter Society (AHS)
Phoenix, Arizona, May 14–17, 2018

National Aeronautics and
Space Administration

Glenn Research Center
Cleveland, Ohio 44135

Acknowledgments

The authors acknowledge the support of the NASA Revolutionary Vertical Lift Technology Project and the technical test support provided by Sigurds Lauge (HX5 Sierra LLC).

This work was sponsored by the Advanced Air Vehicle Program
at the NASA Glenn Research Center

Level of Review: This material has been technically reviewed by technical management.

Available from

NASA STI Program
Mail Stop 148
NASA Langley Research Center
Hampton, VA 23681-2199

National Technical Information Service
5285 Port Royal Road
Springfield, VA 22161
703-605-6000

This report is available in electronic form at <http://www.sti.nasa.gov/> and <http://ntrs.nasa.gov/>

Jetting Phenomenon in Meshed Spur Gears

Irebert Delgado
National Aeronautics and Space Administration
Glenn Research Center
Cleveland, Ohio 44135

Michael Hurrell
HX5 Sierra, LLC
Cleveland, Ohio 44135

Summary

Rotorcraft gearbox transmissions are required to efficiently transfer power from the turbine engine to the main and tail rotor blades. Losses in transmission efficiency impact mission payload and aircraft range. These systems are expected to deliver high power with high gear-pitch-line velocities. More recently, shrouding has been employed to reduce windage power losses (WPLs) associated with the high gear rotational speeds. However, recent experimental results from tests conducted by the authors show the negative impact of close-clearance shrouds on WPL, particularly at the meshed region where flow is ejected, or jetted, from the collapsing tooth spaces. A literature review was conducted to gain further insight into the phenomenon of gear mesh jetting and strategies to mitigate and control the associated losses. An analysis was conducted on windage losses in the mesh region. Test results are given for a modified shroud configuration. Finally, a discussion on observed trends follows with suggestions for future research.

Introduction

Losses in geared systems can be divided into load-dependent and load-independent losses. Load-dependent losses are losses incurred in the gears and bearings that increase proportionally with applied load. Load-independent losses, or spin losses, as described by Kahraman and others in Reference 1, are those losses incurred without an applied load. Gear windage power losses (WPLs) are categorized under spin losses and include losses resulting from (1) viscous drag on the faces of the gear; (2) impingement of the air and oil medium on the gear teeth, also known as pressure torque (Ref. 2); and (3) pumping of the air and oil medium in the intertooth spaces of the gear. High-velocity jetting is believed to occur during the “engaging” portion of the meshing cycle for a pair of spur gear teeth in mesh. In general, WPL has been found to significantly affect gearbox efficiency above 10,000 ft/min (51 m/s) (Refs. 3 to 4).

Researchers have found that the use of shrouding can mitigate viscous and pressure torque drag losses. For spur gears, shrouding involves enclosing the component axially and radially with strategically placed drain holes. Hill (Ref. 2) and others have shown through computational fluid dynamics (CFD) analysis that shrouding acts to preserve the fluid velocity at the vicinity of the rotating gear, resulting in reduced power consumption. In general, WPL is reduced with decreasing clearance between the stationary shroud and the rotating gear. However, recent results from tests conducted on shrouded meshed spur gears by Delgado and Hurrell (Ref. 5) show that the beneficial effects of shrouding may be offset by axial jetting in the vicinity of the gear mesh. Figure 1 shows WPL results for different shroud configurations for a pair of meshed spur gears. The experiment was conducted at the NASA Glenn Research Center gear windage test

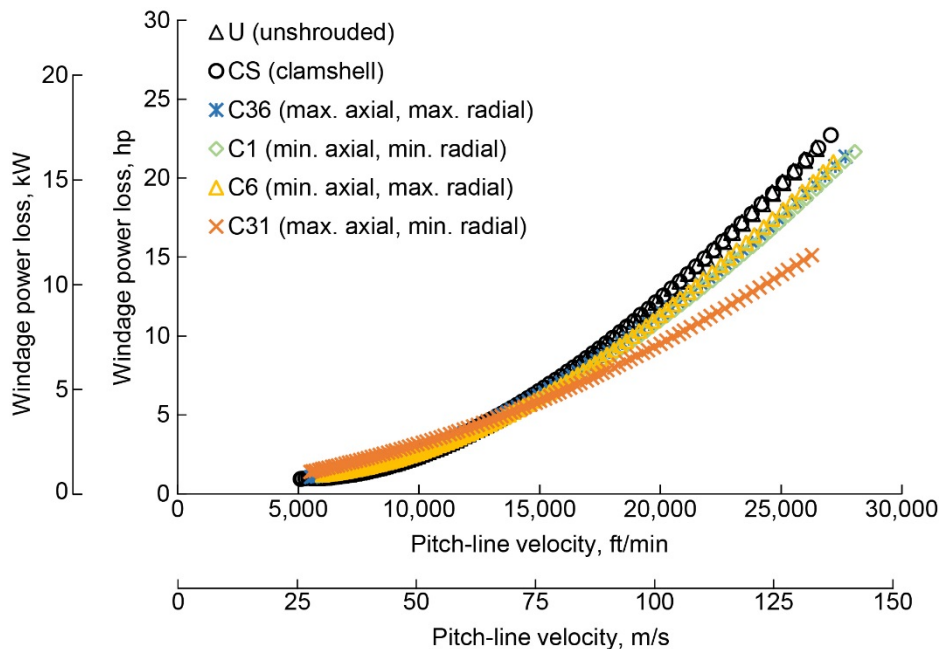


Figure 1.—Comparison of meshed spur gear windage power loss versus shroud configuration clearances for wind-down cycle 3. Brake torque, 10 in.·lb (1.1 N·m).

rig (Figure 2). From previous research, the small axial, small radial clearance configuration should give the largest reduction in WPL. However, the largest reduction in WPL was given by the large axial, small radial clearance configuration. Assuming that jetting exists at the spur gear mesh and was “blocked” by the close-clearance shroud (e.g., small axial, small radial clearance data), the air and fluid medium could be redirected back toward the gear faces as well as the intertooth spaces, thereby increasing WPL.

A literature search was conducted to gain a better understanding of the jetting phenomenon and to investigate how it might be controlled, particularly with the use of shrouding. The search focused on the following questions:

- (1) What is the underlying physical mechanism causing the axial jetting in meshed spur gears?
- (2) What analyses and experiments have been conducted?
- (3) How is jetting related to squeezing and pocketing power losses?
- (4) How is efficiency affected in transmitting power?
- (5) How does axial jetting affect the use of shrouding?

The literature review will be followed by a windage loss analysis and presentation of test results for a modified shroud configuration. A discussion of observed trends and open issues will conclude with suggestions for further work.

Literature Review

In efforts to decrease noise or reduce power losses in geared systems, several researchers have theorized, modeled, or observed the air and oil medium being squeezed out of the spaces between meshed spur gear teeth. Following is a review of the findings of those researchers with emphasis on the questions noted above and, more specifically for this study, how this phenomenon impacts the effectiveness of shrouding in reducing WPL.

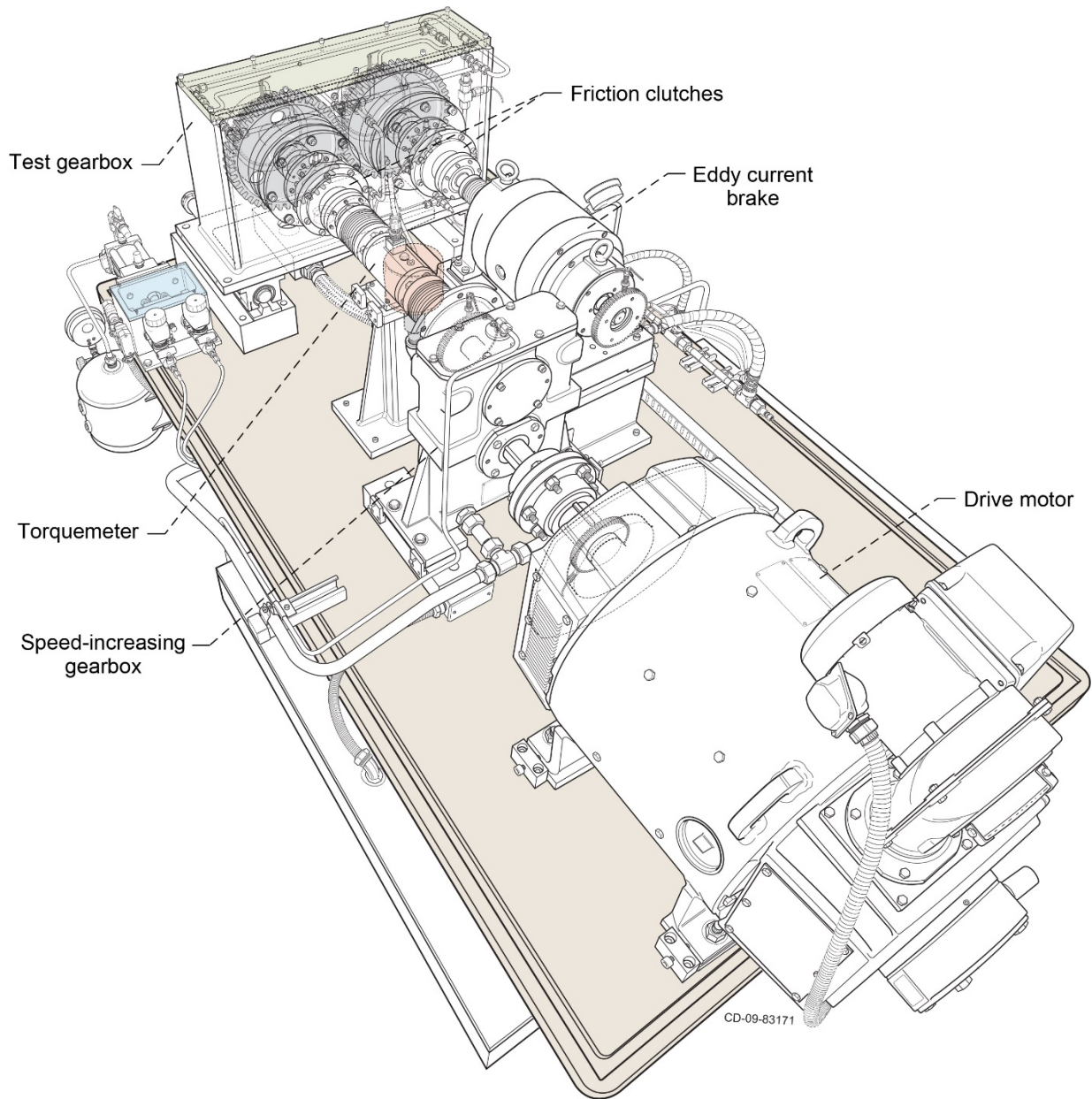


Figure 2.—NASA Glenn Research Center gear windage test rig.

(1) What is the underlying physical mechanism causing the axial jetting in meshed spur gears?

Early acoustic experiments by Rosen (Ref. 6) point to air being forced out of the space between a gear tooth and its mating gear teeth. Dudley (Ref. 7) notes that oil may become trapped in the meshing region, resulting in power loss, and suggests that the effect might be mitigated by allowing for sufficient room within the casing. Wittbrodt and Pechersky (Ref. 8) describe the phenomenon as the air and lubricant in the volume space between mating teeth being compressed and forced out of the sides and between the mating teeth. Diab et al. (Ref. 9) describe the phenomenon as a trapping of the air and oil mixture in the tooth interspaces as it undergoes a compression and expansion within a tooth meshing cycle. The gas can flow in both the axial and radial directions. Seetharaman and Kahraman (Ref. 10) describe the phenomenon as “pocketing,” where the air and oil mixture is treated as a compressible fluid confined by

the cavity formed between a tooth on one gear and the mating space between two adjacent teeth on the opposing gear, or intertooth space. Due to rotation, the volume of air and oil is squeezed, resulting in a higher pressure differential than outside the volume. The mixture is forced out of the ends and backlash regions of the intertooth cavity.

(2) What analyses and experiments have been conducted?

Analyses by Rosen (Ref. 6) calculate air discharge velocities for the spur gear meshing region based on change in volume as the teeth rotate through mesh. Rosen's findings show that the maximum discharge velocity occurred at nearly the same time as the measured maximum acoustic energy. For the gear geometry tested, this maximum velocity occurs approximately 8° before contact at the pitch point. Additionally, it is noted that air is discharged prior to the pitch point and then "sucked in" after the pitch point. Finally, one of the methods used to quiet the gears was to allow a large space at the two ends of the teeth for air and oil to escape. For the gear geometry tested, Rosen calculates discharge velocities approaching sonic conditions.

Work by Ariura et al. (Ref. 11) models power loss due to oil "trapping" and "acceleration." Power loss due to trapping of the oil was found to be significant at flow velocities of 10 to 20 m/s (1,969 to 3,937 ft/min) while power loss values due to circumferential acceleration of the oil were significant at higher velocities. Experimentally, jetted lubricating oil was also observed to flow axially out of the meshing region.

Wittbrodt and Pechersky (Ref. 8) performed a one-dimensional incompressible and compressible flow analysis that shows higher fluid flow at the gear tooth tips compared to axial flow at the ends of the gear teeth. Fluid velocities may reach sonic conditions and are dependent on rotational speed and relative gear geometries. Peak velocities are shown to occur prior to the gear teeth reaching their pitch point in the meshing cycle; this timing again varies with geometry. Regarding the specific rotational position of maximum end flow, positive or negative, Wittbrodt and Pechersky's analysis provides a number of factors that affect this location. Higher pitch-line velocities, smaller backlash, and larger gear ratio tend to move the maximum velocity earlier in the meshing cycle. One particularly interesting result shows nondimensional velocity going to zero just after the pitch point. Recall that Rosen's work shows air velocities becoming negative after the pitch point, indicating a reversal in fluid flow from expulsion to ingestion. While Wittbrodt and Pechersky do not explicitly discuss this, several other researchers (Refs. 6, 9, and 10) report negative fluid velocities after the meshing spur gears pass the pitch point (i.e., fluid ingestion into the gear tooth spaces). Additional trends from Wittbrodt and Pechersky's analysis include the following:

- (1) Tooth flow velocities are generally higher than end-flow velocities.
- (2) End flow tends to dominate narrow-face-width gears.
- (3) Higher fluid velocities result from spur gears with ratios closer to unity.
- (4) Higher fluid velocities result from smaller backlash.
- (5) Higher fluid velocities result from higher pitch-line velocities.
- (6) Higher pitch-line velocities shift the peak fluid velocity (possibly sonic) to earlier in the meshing cycle.

Using conservation of momentum principles, Seetharaman and Kahraman (Ref. 9) calculate discharge velocities at the ends and backlash regions of mating spur gear teeth. Results show that end-flow power loss increases with respect to backlash power loss as face width increases, corroborating findings by

Wittbrodt and Pechersky (Ref. 8). Analyses show a maximum positive velocity (i.e., expulsion) prior to the pitch point and a maximum negative velocity (i.e., suction) after the pitch point. The absolute magnitude of these velocities increases with increasing pitch-line velocity. For the unity ratio gears analyzed, end-flow pressures increased with increasing velocity. End-flow pressure magnitudes were slightly less than the magnitudes of the backlash pressure. Correspondingly, end-flow velocities were slightly lower than backlash flow velocities for a given rotational position.

A CFD analysis in a fully immersed lubricating fluid by Concli and Gorla (Ref. 12) shows that the axial velocity at the gear mesh is maximum in the middle of the width of the tooth and decreases rapidly toward the end (opening) of the mating teeth.

Al et al. (Ref. 13) perform a single-phase two-dimensional modeling study on meshed spur gears. The mesh between the gear teeth is modeled as they go into and out of mesh. Contact between the gear teeth is not modeled. Axial flows are not considered in the model. Results support the existence of a maximum positive pressure prior to the meshing pitch point. The results also support that a period of expulsion (positive flow) exists prior to the meshing pitch point, followed by a period of suction (negative flow) after the meshing pitch point. Results are in agreement with experimental data by Diab et al. (Ref. 9).

Burberi et al. (Ref. 14) simulate meshed spur gears rotating in a submerged oil with the flow modeled as isothermal and incompressible. A dynamic mesh, moving boundary approach is used with gear teeth not in contact (i.e., 2/3 element fluid layer). Results are comparable with experiments by Gorla et al. (Ref. 15). Results show oil flow moving out of and into mesh.

Experimental and analytical work by Diab et al. (Ref. 9) shows a positive increase in pressure at the root of the gear teeth during meshing but a rotational angle before the pitch point. This is followed by a decrease in pressure (i.e., suction) after the pitch point. The analysis and observations are in line with those of Rosen (Ref. 6), Wittbrodt and Pechersky (Ref. 8), and Seetharaman and Kahraman (Ref. 10).

Particle image velocimetry (PIV) studies by Hartono et al. (Refs. 16 and 17) for meshed spur gears at different levels of oil immersion show recirculation of fluid flow that impinges on the sides and faces of the gear teeth. Pitch-line velocities were limited to less than 20 m/s (3,937 ft/min). Visual analysis in a fully immersed condition at 0.55 m/s (108 ft/min) and 1.1 m/s (217 ft/min) gear pitch-line velocity indicated fluid movement into mesh. The particle trajectories, or streamlines, in the vicinity of the meshing region show an axially outward flow that increases in intensity with pitch-line velocity.

As shown in Figure 1, Delgado and Hurrell (Ref. 5) observe that the maximum axial, minimum radial shroud configuration gives a lower WPL than the minimum axial, minimum radial shroud configuration. One possible reason for this result is the recirculation back into the meshing/rotational region of the axial jetting mixture.

(3) How is jetting related to squeezing and pocketing power losses?

For the purposes of this study, jetting is the axial flow of fluid resulting from the squeezing, or pocketing, of that fluid mixture (air and oil) in the volumetric interspaces of the meshed spur gears. Generally, jetting occurs in the first half of the meshing cycle between a pair of mating spur gear teeth prior to those teeth reaching the pitch point. For compressible fluids, the sharp decrease in volumetric space results in an expulsion of fluid axially out of the ends of the meshed spur gear teeth and radially through the backlash region. The compression of fluid and flow out of the volume results in power loss. Jetting and the associated power loss can be affected by the placement of axial shrouds.

(4) How is efficiency affected in transmitting power and (5) How does axial jetting affect the use of shrouding?

Several researchers (Refs. 3 to 5) have noted that WPL becomes increasingly problematic above 10,000 ft/min (51 m/s). The authors' use of shrouds in Reference 18 was shown to decrease WPL for meshed spur gears. Analyses by researchers at The Pennsylvania State University (Ref. 2) show the largest decrease in WPL for single spur gears using shrouds at close clearance. Although the use of close-clearance shrouds for meshed spur gears resulted in a decrease in WPL, it did not translate into the largest decrease in WPL. The largest decrease in WPL was observed using the large axial, small radial shroud configuration (Figure 1). Comparing this data with PIV data by Hartono et al. (Refs. 16 and 17) as well as analyses on the jetting phenomenon from several researchers, we conclude that axial jetting would need to be better controlled, particularly at high speeds. Table I summarizes the analyses and experiments found regarding the axial jetting phenomenon.

Analysis of Literature Survey

Analyses by Rosen (Ref. 6), Wittbrodt and Pechersky (Ref. 8), and Seetharaman and Kahraman (Ref. 10) indicate that a maximum positive end-flow velocity is attained before the teeth of two meshed spur gears reach the pitch point in the meshing cycle. This is followed by a maximum negative end-flow velocity after reaching the pitch point (Figure 3 and Figure 4). Experimental work by Diab et al. (Ref. 9) corroborates these findings through experimental observation. The trapped volume between the meshed gears decreases to a minimum at the pitch point, then expands afterwards. For incompressible flows, Wittbrodt and Pechersky (Ref. 8) found that the highest fluid velocities occurred when discharge areas, end flow or tooth flow, were minimal and volume changes with respect to rotational position were maximized. A number of results indicate discharge velocities approaching sonic conditions.

TABLE I.—SUMMARY OF DATA SOURCES FOR AXIAL JETTING PHENOMENON

Source	Analytical	Experimental	Notes
Rosen (Ref. 6)	Change in volume	Acoustic, noise	
Ariura et al. (Ref. 11)	NA	Axial jetting observed via stroboscope	
Wittbrodt and Pechersky (Ref. 8)	One-dimensional incompressible and compressible	NA	
Seetharaman et al. (Ref. 10)	Closed-form, compressible, physics-based	Compare to data from Reference 19	Single-phase fluid
Concli and Gorla (Ref. 12)	Three-dimensional (3D) computational fluid dynamics (CFD), volume of fluid	NA	Oil bath, no tooth contact
Al et al. (Ref. 13)	Two-dimensional CFD	NA	Single-phase, no tooth contact
Burberi et al. (Ref. 14)	3D CFD, incompressible	NA	
Diab et al. (Ref. 9)	Isentropic, numerical	Gear tooth root pressure measurement	Air only
Hartono et al. (Refs. 16 and 17)	NA	Particle image velocimetry	
Delgado and Hurrell (Ref. 5)	NA	Gear windage power loss	

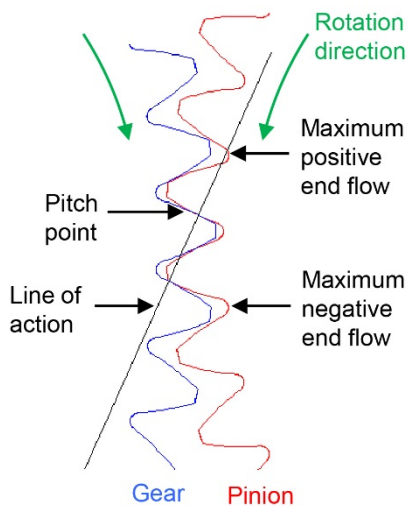


Figure 3.—Relative positions of maximum positive and negative end flow per literature review for meshed spur gears.

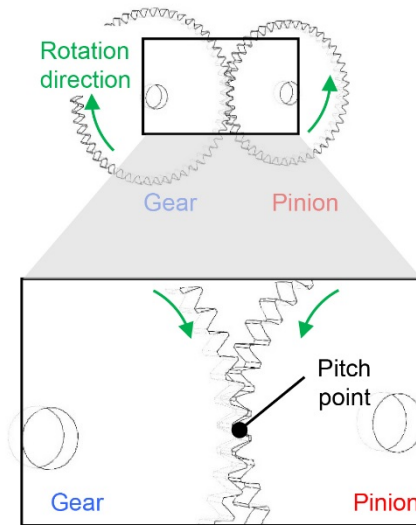


Figure 4.—Meshed spur gears showing trapped volume decreasing and increasing in magnitude before and after pitch point.

Although the Hartono research (Refs. 16 and 17) did not specifically show an axial jetting fluid flow component, the increased outward bow around the meshing region when comparing the data at 0.55 m/s (108.3 ft/min) and 1.1 m/s (216.5 ft/min) may be an indication of increased influence of that phenomenon on the local flow field. This agrees with previous research findings that axial jetting velocities increase with increasing pitch-line velocities. Given that the authors conducted WPL tests with jet-lubricated gears at pitch-line velocities near 150 m/s (29,500 ft/min), the axial jetting velocities could be substantial.

Nearly all of the research noted above indicates that maximum end-flow velocities were attained prior to reaching the pitch point for any pair of meshed spur gear teeth in the meshing cycle. An open question is where that maximum velocity is attained relative to the “center distance” direction between meshed spur gears. For involute gear tooth profiles, the line of action is a straight line, as shown in Figure 3, and defines the tooth contact for the entire meshing cycle for a pair of spur gear teeth. Also, depending on the gear rotation, the line of action is skewed either to the right or left relative to center. These observations should be accounted for, assuming close-clearance shroud designs are diverting the air and lubricant flow back to the meshing and rotational regions. Note also that for noninvolute gear tooth profiles the line of action may be an S-curve (Ref. 20). A number of researchers have also noted a suction effect after any pair of meshed spur gears have reached the pitch point. The end flow is reversed, going into mesh instead of out of mesh. Its effect on WPL, if any, is unknown, with or without shrouding.

In terms of exit velocities, analyses by Rosen (Ref. 6) and Wittbrodt and Pechersky (Ref. 8) for their particular meshed spur gear geometries show axial velocities approaching sonic conditions. In addition, higher pitch-line velocities result in the exit velocity reaching sonic conditions earlier in the meshing cycle. Higher pitch-line velocities are also known to increase WPL.

A number of researchers show backlash velocities slightly higher than end-flow velocities. The effect of the backlash flow velocity on WPL is unknown. It may be reasonable to assume that any type of air and oil flow back into the meshing region would have a negative effect on WPL. Modeling and experiments using a shroud design that blocks the suction flow into the gear mesh would improve understanding of the flow in this portion of the meshing cycle. Given findings that exit flows reach nearly sonic conditions, combined with visualization studies by Hartono (Refs. 16 and 17), further analyses and

experiments are needed to determine if the flow is axially straight relative to the meshing region or, alternatively, if its direction is dependent on rotational speed, gear tooth geometry, or some other factor.

Although the Hartono research was done at relatively low pitch-line velocities, the visualization results indicate fluid flow near the meshing region as axially outward and down (i.e., toward the out-of-mesh region). The direction of the fluid flow was, up to this point, assumed to be axially outward and orthogonal to the meshing region. Additional work is needed to corroborate these results.

Pocketing Calculation

Referring to the recent results from tests conducted on shrouded meshed spur gears (Ref. 5), an analysis was conducted to determine the power loss due to pocketing of the test gears. The test results indicate that axial shrouding may have an adverse effect on WPL as a result of pocketing and associated axial jetting in the vicinity of the gear mesh. The literature suggests an approach to estimating the power loss associated with pocketing (Refs. 6, 8, 9, and 10). The approach involves defining the control volume created by the meshing action and applying the conservation laws to the control volume at time instants during the mesh cycle.

During the first half of the mesh cycle, the meshing action creates pockets of trapped volume that contain a mixture of air and oil. The trapped volumes decrease in size and shape during the first half of the mesh cycle. The decreasing volume results in flow axially out of the two ends of the volume and radially through the space created by the backlash of the mating gears. Since the loss mechanism associated with the end flow is closely affected by the positioning and configuration of axial shrouds, the proceeding analysis focuses on that portion of pocketing power loss attributed to end flow, i.e., axial jetting.

Following the volume created by the tooth space on the driven gear and the mating tooth of the drive gear, two control volumes can be defined at time t_1 and time t_2 , as shown in Figure 5. Two corresponding volumes are formed by the tooth space on the drive gear and the mating tooth of the driven gear (not shown). The volume changes shape and size as the mesh cycle progresses. The volume size decreases as the two gears proceed through the mesh cycle and reaches a minimum at the pitch point. After the pitch point, the volume begins to increase until the two gears proceed out of mesh.

Referring to the first half of the mesh cycle where the volume is decreasing, the control volumes ($V^{(1)}$, $V^{(2)}$) and flow areas for times t_1 and t_2 are defined as shown in Figure 6.

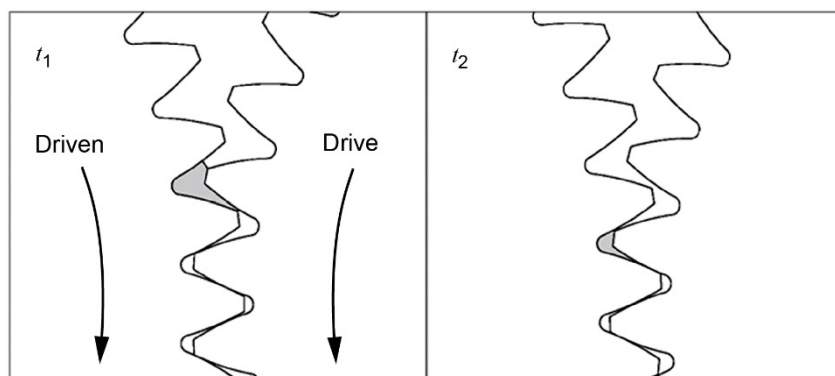


Figure 5.—Control volume change from time t_1 to t_2 during the meshing cycle.

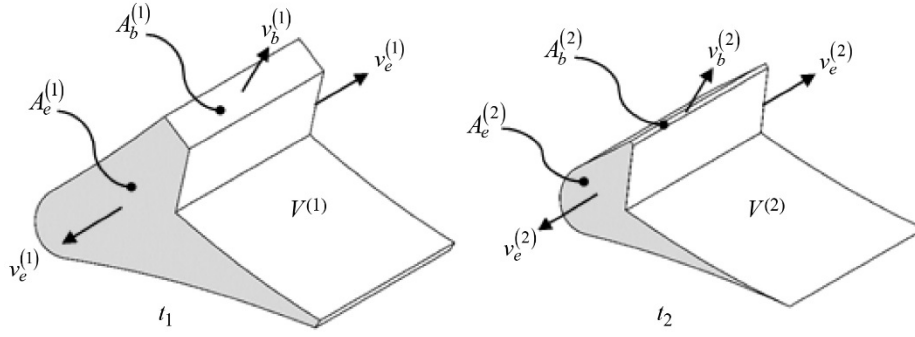


Figure 6.—Control volume V at times t_1 and t_2 . Backlash area and end areas at time i , $A_b^{(i)}$ and $A_e^{(i)}$; backlash velocity and end velocities at time i , $v_b^{(i)}$ and $v_e^{(i)}$.

The backlash area and end areas at time i are given as $A_b^{(i)}$ and $A_e^{(i)}$, respectively. Likewise, the backlash velocity and end velocities are $v_b^{(i)}$ and $v_e^{(i)}$. From conservation of mass, the time rate of change of mass in the control volume plus the net mass efflux crossing the control surface is zero.

$$\frac{d}{dt} \dot{\rho}_{cv} r_{cv} dV + \dot{\rho}_{cs} r_{cs}^* ndA = 0 \quad (1)$$

Proceeding from time t_1 to time t_2 , this relation can be discretized with respect to time.

$$\frac{1}{Dt} \dot{\rho}_{cv}^{(2)} V^{(2)} - r_{cv}^{(1)} V^{(1)} \dot{\rho}_{cv} + 2r_e^{(1)} v_e^{(1)} A_e^{(1)} + r_b^{(1)} v_b^{(1)} A_b^{(1)} = 0 \quad (2)$$

The control volume density and the densities at the backlash area and end areas at time i are given by $\rho_{cv}^{(i)}$, $\rho_b^{(i)}$, and $\rho_e^{(i)}$. Rearranging shows that the velocities are related to the change in volume from t_1 to t_2 .

$$2r_e^{(1)} v_e^{(1)} A_e^{(1)} + r_b^{(1)} v_b^{(1)} A_b^{(1)} = - \frac{1}{Dt} \dot{\rho}_{cv}^{(2)} V^{(2)} - r_{cv}^{(1)} V^{(1)} \dot{\rho}_{cv} \quad (3)$$

Assuming the backlash velocity is proportional to the end velocity

$$v_b = a v_e \quad (4)$$

where a is the proportionality constant and the time increment Dt from t_1 to t_2 is related to the gear surface speed v_s

$$Dt = \frac{Dq}{w} = \frac{r Dq}{v_s} \quad (5)$$

then Equation (3) can be rewritten for the end velocity.

$$v_e^{(1)} = - \frac{v_s}{r Dq} \frac{\dot{\rho}_{cv}^{(2)} V^{(2)} - r_{cv}^{(1)} V^{(1)} \dot{\rho}_{cv}}{\dot{\rho}_{cv} \dot{\rho}_{cv} + 2r_e^{(1)} A_e^{(1)} + a r_b^{(1)} A_b^{(1)}} \quad (6)$$

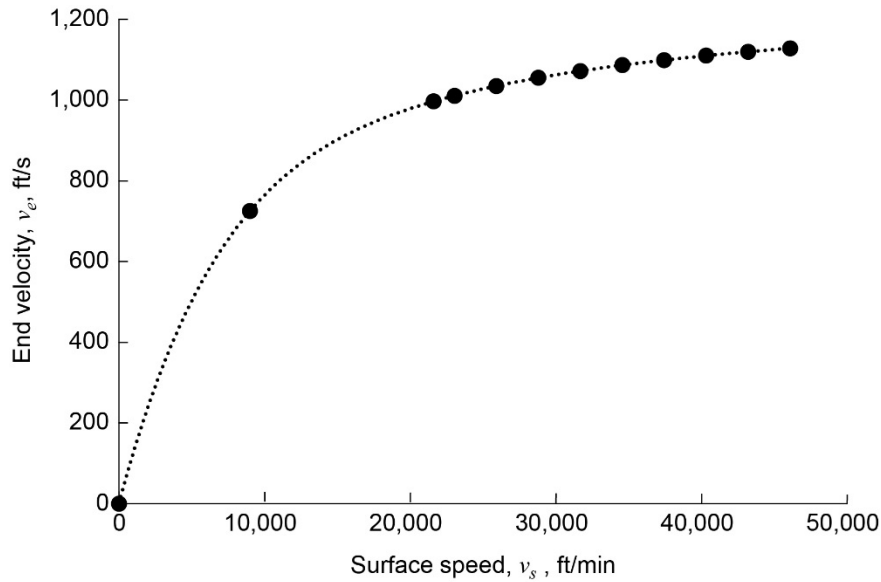


Figure 7.—End velocity v_e versus surface speed v_s at 25 percent mesh for NASA spur gears.

The gear angular speed, the angular increment from t_1 to t_2 , and the gear pitch radius are given by ω , Dq , and r , respectively. Note that the end and backlash velocities are relative velocities because the frame of reference is rotating with the gear.

As shown in Equation (6), the end velocity is nonlinearly related to the surface speed of the mating gears. Using the relations above, the end velocities for the NASA test spur gears were calculated for various pitch-line velocities up to 46,077 ft/min (234 m/s) corresponding to the maximum test rig speed of 16,000 rpm (1,676 rad/s). The results of these calculations for a particular angular position that corresponds to the first quarter of the mesh cycle are shown in Figure 7. Results for the NASA test gears show that by the time one-quarter of the mesh cycle is complete, the end velocity reaches sonic velocity at a surface speed of 46,077 ft/min. In addition, the relations above show that an increase in pitch-line velocity results in a decrease in the time to reach sonic end velocity and, correspondingly, an earlier occurrence of sonic end velocity in the mesh cycle.

From conservation of linear momentum, the total force acting on the control volume is the time rate of change of linear momentum within the control volume plus the net efflux of linear momentum crossing the control volume surface.

$$\dot{\mathbf{a}} \mathbf{F} = \frac{d}{dt} \dot{\mathbf{Q}}_{cv} \mathbf{r}_{cv} v_{cv} dV + \dot{\mathbf{Q}}_{cs} \mathbf{r}_{cs} v_{cs} v_{cs}^* n dA \quad (7)$$

The force acting on the volume end areas is related to the end velocity

$$F_e = r_e (v_e)^2 A_e \quad (8)$$

Because there are two end areas, the power loss due to axial jetting is given as

$$P_e = 2v_e F_e \quad (9)$$

and substituting Equation (8) gives

$$P_e = 2r_e (v_e)^3 A_e \quad (10)$$

The pocketing power loss due to axial jetting varies with the end velocity cubed. For high pitch-line velocities, the end velocity can approach the speed of sound.

Seetharaman and Kahraman (Ref. 10) break the total WPL of two spur gears in mesh into two components: pumping loss due to pocketing P_p and loss due to drag P_d .

$$P_w = P_p + P_d \quad (11)$$

The pumping power loss due to pocketing is further subdivided into the power loss from end flow P_e and power loss from backlash flow P_b . Seetharaman and Kahraman also divide the drag component into two subcomponents: drag on the drive gear P_{d1} and drag on the driven gear P_{d2} . Calculations of the pocketing power loss at drive gear surface speeds in excess of 25,000 ft/min (127 m/s) for the NASA test gears and test results for different shroud configurations of both single and meshed spur gears (Ref. 5) indicate that a large portion of the total WPL is unaccounted for based on the pocketing and drag formulations defined above. Percentages of the total power loss at 25,000 ft/min for the unshrouded meshed spur gear test (largest radial and largest axial shroud clearance) and the C1 shroud configuration meshed spur gear test (smallest radial and smallest axial shroud clearance) reported in Reference 5 are shown in Figure 8 and Figure 9, respectively. Seetharaman and Kahraman report a similar discrepancy between predicted and experimental total WPL at higher gear speeds.

A comparison of results from testing conducted at NASA of shrouded single spur gears (Figure 10) and meshed spur gears (Figure 11) indicates that there may be a third subcomponent of drag related to the interaction of the two gears in the vicinity of the mesh region, P_{d12} .

$$P_d = P_{d1} + P_{d2} + P_{d12} \quad (12)$$

The flow in this region is highly turbulent and is the result of the impingement of the flows attached to the two gears as they rotate in opposing directions.

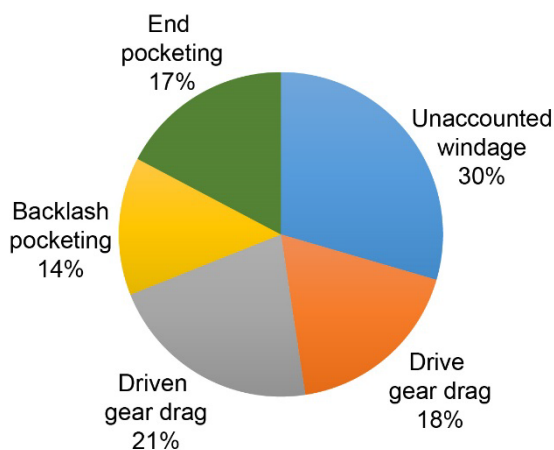


Figure 8.—Total windage loss component percentages for unshrouded test condition (largest radial and largest axial shroud clearance) at 25,000 ft/min (127 m/s) drive gear surface speed.

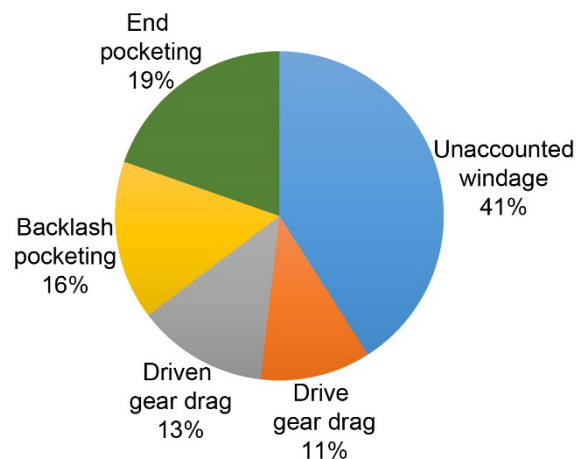


Figure 9.—Total windage loss component percentages for the C1 shroud configuration (smallest radial and smallest axial shroud clearance) at 25,000 ft/min (127 m/s) drive gear surface speed.

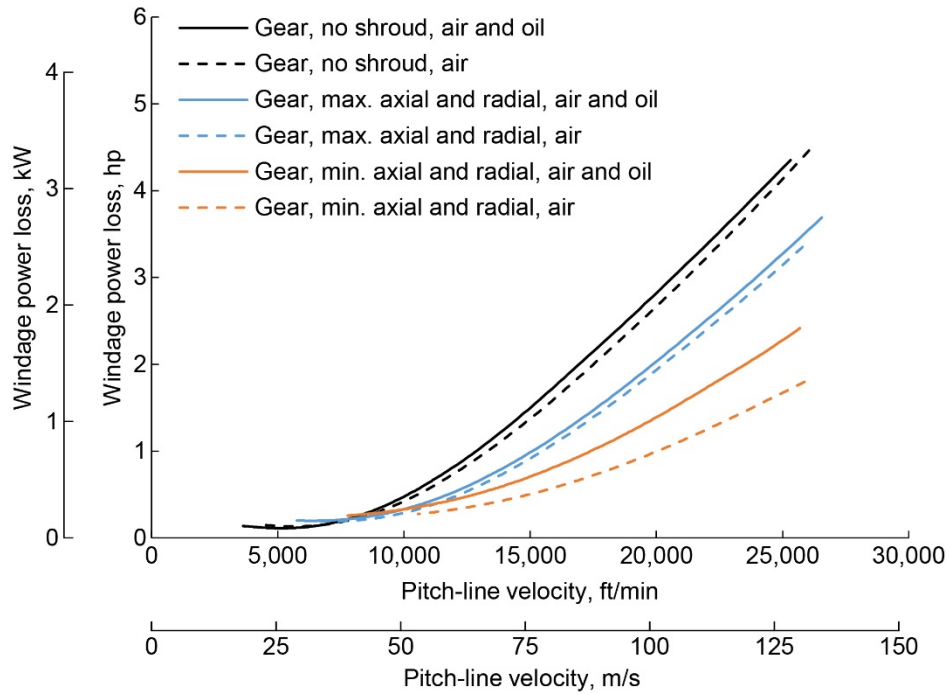


Figure 10.—Single spur gear windage power loss data for various shroud configurations.

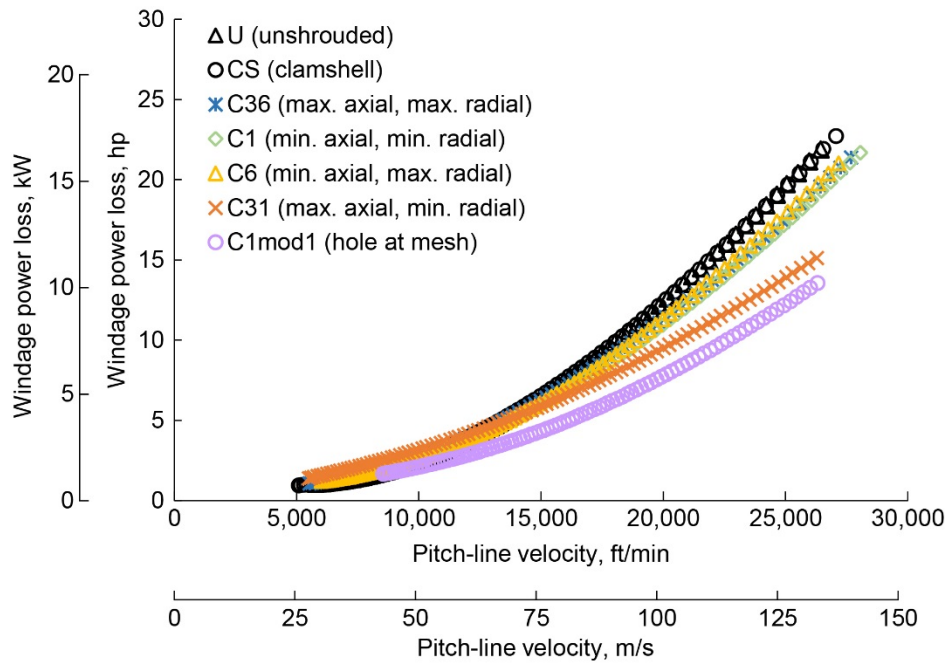


Figure 11.—Meshed spur gear windage power loss data for various shroud configurations.

Hill (Ref. 2) performed a CFD analysis of the NASA spur gears and observed vortices in the tooth space of the gears when enclosed in a radial shroud. This secondary flow may be another mechanism of loss contributing to total WPL. The vortices in the tooth space are similar to the flow within the flow passages of a periphery, or regenerative, pump. A regenerative pump is used in large-head, small-flow

applications that are not suited for the traditional centrifugal or positive displacement pump (Ref. 21). The testing conducted at NASA indicates that this secondary flow may be present for the case of tight-clearance radial shrouding. As a result, a third component can be added to the loss due to pocketing: P_s , pumping power loss due to this secondary flow within the gear tooth space for close radial shrouding.

$$P_p = P_e + P_b + P_s \quad (13)$$

The NASA tests (Ref. 5) indicate that closely conforming axial and radial shrouds can reduce total WPL. However, these tests also indicate that an optimized shroud configuration requires a closer examination of the component loss mechanisms that contribute to the total WPL to determine how these mechanisms are affected by shrouding. For instance, close axial shrouds may help in reducing drag loss on the sides of the gears, but they may increase losses due to pocketing. Close-clearance axial shrouds may act to reduce the flow through the two end areas A_e , forcing more of the compressed pocket volume to squeeze through the smaller backlash area A_b , resulting in an increase in pocketing loss. For close-clearance radial shrouds, the study by Hill (Ref. 2) shows the presence of secondary flows within the tooth spaces of the NASA spur gears. This secondary flow may contribute to the overall pumping power loss when close radial shrouding is utilized. The NASA tests are inconclusive with regard to the effect of shrouding on the drag loss associated with the interaction of two gears in mesh, P_{d12} . This loss mechanism may follow the same trend as the individual gear drag loss components P_{d1} and P_{d2} , i.e., decreasing with decreasing shroud clearance. In general, all of the loss components increase with increasing pitch-line velocity, so understanding the component mechanisms of WPL is critical for the high-speed gear trains of modern rotorcraft applications.

Modified Shroud Test Results

Based on the literature review and analysis of the pocketing losses, a WPL test was conducted using shrouds modified with cutouts near the meshing region. Figure 11 shows WPL versus pitch-line velocity data for meshed spur gear tests at various shroud configurations. Previous work by the authors (Ref. 5) had shown that the C31 configuration (max. axial, min. radial) condition had given the largest decrease in WPL of 29 percent at a pitch-line velocity of 25,000 ft/min (127 m/s) relative to the unshrouded configuration. The C1 configuration (min. axial, min. radial) decreased WPL by only 13 percent. Now included in the dataset is WPL data for a modified shroud configuration, C1mod1, containing square openings at both ends of the meshing spur gears. Compared with the unshrouded configuration at the same pitch-line velocity, a 38 percent reduction in WPL is observed. The axial and radial locations are the same for the C1 and the C1mod1 configuration with the exception of the square-hole cutouts for the C1mod1 configuration. Results of the modified shroud with cutouts are indicative of the negative effects of axial jetting. More work is needed to understand axial jetting and how best to mitigate its effect on WPL.

Concluding Remarks

Results of the literature review showed several analyses and experiments indicating the presence of axial jetting. Although highly dependent on factors such as gear geometry and pitch-line velocity, there was general agreement that axial jetting was found to occur prior to the pitch point and could reach sonic conditions. In addition, a “suction” action occurs after reaching the pitch point in the meshing cycle. Its effect on windage power loss (WPL) is unknown, as is its effect on shrouding.

A comparison of pocketing analysis data with NASA WPL data found two potential additional components to WPL: (1) an interaction between the meshing spur gears and (2) a recirculation of the fluid within the interspaces of the gear teeth.

The initial test results for the modified shroud configuration are promising. A 38 percent reduction in WPL was observed compared with the unshrouded configuration. This is an improvement over the 29 percent WPL reduction for the maximum axial, minimum radial shroud configuration. Results are indicative of the effect of jetting in the meshing region. Further analysis on the C1mod1 shroud configuration is necessary to optimize the design. Based on the literature and results from the authors' tests, a number of design guidelines would aid the shroud optimization. These guidelines would apply for pitch-line velocities higher than 10,000 ft/min (51 m/s):

1. To the degree possible, avoid recirculation of the air and oil mixture in the meshing region.
2. For spur gears, allow a means for the fluid flow to exit the meshing region in the axial direction.
3. Allow lubricant to cool and lubricate quickly and to exit the meshing region as quickly as possible.
4. Position the oil drains in the gearbox to allow for the quick exit of the lubricant.

A fluid dynamics model of the gearbox using shrouds at running condition could potentially show the magnitude and direction of the fluid flow and impingement of the air and oil mixture on the gear teeth. Given these results, appropriate shroud modifications could be made that inhibit the air and oil mixture from recirculating back into the gear mesh, teeth, and gear sides. Again, the objective is to limit the fluid to lubrication and cooling of the gears.

Experimental efforts are underway at the NASA Glenn Research Center Gear Windage Test Facility to determine the areas of maximum expulsion and suction of the air and lubricant mixture for the spur gears tested by the authors. Dynamic pressure sensors will be placed next to the spur gear meshing region to triangulate the regions of maximum and minimum pressure. This data will be used to determine end-flow velocities. Depending upon the confidence of measurements, a pressure profile map could be generated to further aid in understanding the effectiveness of close-clearance shrouds.

In addition, a feasibility study is planned of particle image velocimetry (PIV) tests of jet-lubricated gears at pitch-line velocities greater than 50 m/s (9,843 ft/min). Visual data of this kind, even without shrouding, would greatly increase understanding of the effect of fluid flow within a gearbox in relation to windage power losses.

References

1. Kahraman, A.; Hilty, D.R.; and Singh, A.: An Experimental Investigation of Spin Power Losses of a Planetary Gear Set. *Mech. Mach. Theory*, vol. 86, 2015, pp. 48–61.
2. Hill, Matthew J.; and Kunz, Robert F.: A Computational Investigation of Gear Windage. NASA/CR—2012-217807, 2012. <http://ntrs.nasa.gov>
3. Townsend, Dennis P.: *Dudley's Gear Handbook*. McGraw-Hill, New York, NY, 1991.
4. Diab, Y., et al.: Windage Losses in High Speed Gears—Preliminary Experimental and Theoretical Results. *J. Mech. Des.*, vol. 126, no. 5, 2004, pp. 903–908.
5. Delgado, I.R.; and Hurrell, M.J.: The Effectiveness of Shrouding on Reducing Meshed Spur Gear Power Loss Test Results. Presented at the AGMA Fall Technical Meeting, Columbus, OH, 2017.
6. Rosen, Moe William: Noises of Two Spur-Gear Transmissions. *Noise Control*, vol. 7, no. 6, 1961, pp. 11–19.
7. Dudley, Darle W.: *Gear Handbook: The Design, Manufacture, and Application of Gears*. McGraw Hill Book Company, New York, NY, 1962.

8. Wittbrodt M.J.; and Pechersky, M.J.: A Hydrodynamic Analysis of Fluid Flow Between Meshing Spur Gear Teeth. The Pennsylvania State University Applied Research Lab, Technical Report No. TR 87-006, 1987.
9. Diab, Y., et al.: Experimental and Numerical Investigations on the Air-Pumping Phenomenon in High-Speed Spur and Helical Gears. *J. Mech. Eng. Sci.*, vol. 219, no. 8, 2005, pp. 785–800.
10. Seetharaman, Satya; and Kahraman, Ahmet: A Windage Power Loss Model for Spur Gear Pairs. *Tribol. T.*, vol. 53, no. 4, 2010, pp. 473–484.
11. Ariura, Yasutsune, et al.: The Lubricant Churning Loss in Spur Gear Systems. *B. JSME*, vol. 16, no. 95, 1973, pp. 881–892.
12. Concli, F.; and Gorla, C.: Oil Squeezing Power Losses in Gears: A CFD Analysis. *WIT Trans. Eng. Sci.*, vol. 74, 2012, pp. 37–48.
13. Al, Baydu C.; Simmons, Kathy; and Morvan, Herve P.: Computational Investigation of Flows and Pressure Fields Associated With Spur Gear Meshing. *ASME GT2014-26145*, 2014, p. V05CT16A023.
14. Burberi, E., et al.: CFD Simulations of a Meshing Gear Pair. *ASME GT2016-57454*, 2016, p. V05AT15A024.
15. Gorla, Carlo, et al.: Hydraulic Losses of a Gearbox: CFD Analysis and Experiments. *Tribol. Int.*, vol. 66, 2013, pp. 337–344.
16. Hartono, Erwin Adi; Golubev, Maxim; and Chernoray, Valery: PIV Study of Fluid Flow Inside a Gearbox. 10th International Symposium on Particle Image Velocimetry, Delft, The Netherlands, 2013.
17. Hartono, E.A.; Pavlenko, A.; and Chernoray, V.: Stereo-PIV Study of Oil Flow Inside a Model Gearbox. Presented at the 17th International Symposium on Application of Laser Techniques to Fluid Mechanics, Lisbon, Portugal, 2014, p. 3.8.3.
18. Delgado, Irebert R.; and Hurrell, Michael J.: Experimental Investigation of Shrouding on Meshed Spur Gear Windage Power Loss. *NASA/TM-2017-219536*, 2017. <http://ntrs.nasa.gov>
19. Petry-Johnson, T.T., et al.: An Experimental Investigation of Spur Gear Efficiency. *J. Mech. Des.*, vol. 130, no. 6, 2008, p. 062601.
20. Merritt, Henry Edward: *Gear Engineering*. John Wiley & Sons, New York, NY, 1971.
21. Engeda, Abraham; and Raheel, Mukarrum: Theory and Design of the Regenerative Flow Compressor. *IGTC 2003 Tokyo TS-050*, 2003.

